



HAL
open science

Wideband magnetic losses and their interpretation in HGO steel sheets

O. de la Barrière, E. Ferrara, A. Magni, A. Sola, C. Ragusa, C. Appino, F. Fiorillo

► **To cite this version:**

O. de la Barrière, E. Ferrara, A. Magni, A. Sola, C. Ragusa, et al.. Wideband magnetic losses and their interpretation in HGO steel sheets. *Journal of Magnetism and Magnetic Materials*, 2023, 565, pp.170214. 10.1016/j.jmmm.2022.170214 . hal-03912960

HAL Id: hal-03912960

<https://hal.science/hal-03912960v1>

Submitted on 26 Dec 2022

HAL is a multi-disciplinary open access archive for the deposit and dissemination of scientific research documents, whether they are published or not. The documents may come from teaching and research institutions in France or abroad, or from public or private research centers.

L'archive ouverte pluridisciplinaire **HAL**, est destinée au dépôt et à la diffusion de documents scientifiques de niveau recherche, publiés ou non, émanant des établissements d'enseignement et de recherche français ou étrangers, des laboratoires publics ou privés.

Wideband magnetic losses and their interpretation in HGO steel sheets.

O. de la Barrière^{a*}, E. Ferrara^b, A. Magni^b, A. Sola^{b*}, C. Ragusa^c, C. Appino^b, F. Fiorillo^b

^aLaboratoire SATIE, CNRS-ENS, Saclay, France

^bAdvanced Materials Metrology and Life Sciences, Istituto Nazionale di Ricerca-Metrologica-INRIM, 10135 Torino, Italy

^cEnergy Department, Politecnico di Torino, 10129 Torino, Italy

1
2
3
4
5
6
7
8
9

*Corresponding author

e-mail: Olivier.DE-LA-BARRIERE@ens-cachan.fr

HIGHLIGHTS

- A broadband investigation (1 Hz-10kHz) on the loss properties and domain dynamics on HGO Fe-Si. Role of the sheet thickness (conventional 0.29 mm vs. novel 0.18 mm thick laminations).
- Fluxmetric measurements of hysteresis loops and losses are associated with dynamic high-speed Kerr imaging of the domain structure.
- Modeling of loss versus frequency made by keeping into account deep skin effect. It relies on the calculation of the classical loss component by a numerical approach with the material constitutive equation provided by the normal DC magnetization curve. The loss decomposition is made up to 10 kHz. It shows the vanishing contribution of the dw generated losses at the highest frequencies.
- The dynamic response of the array of 180° dws is treated starting from the concept of dw bowing. The dw configuration along the magnetization cycle and its evolution with frequency are obtained by numerical modeling, including wall merging and transition from low-frequency back-and-forth oscillation (mode 1) to high-frequency transformation into horizontal saturated bands sweeping from surface to the inner demagnetized core (mode 2).

64
65
66
67
68
69
70
71
72
73
74
75
76
77
78
79
80
81
82

Abstract

The magnetic properties of high-permeability grain-oriented (HGO) Fe-Si sheets have been investigated in the frequency range 1 Hz-10 kHz, with attention devoted to the role of thickness on the behavior of the magnetic losses and the phenomenology of skin effect. The study is focused on the wideband response of 0.174 mm and 0.289 mm thick sheets, comparatively tested at peak polarization values ranging between 0.25 T and 1.7 T. The experiments associate the fluxmetric measurements with direct Kerr observations of the dynamics of the domain walls. A picture of the magnetization process comes to light, where the dynamics of the flux reversal takes hold under increasing frequencies through the motion of increasingly bowed 180° walls, eventually merging at the sheet surface for a fraction of the semi-period. This effect can be consistently predicted, starting from the Kerr-based knowledge of the equilibrium wall spacing, by the numerical modeling of the motion of an extended array of 180° domain walls, subjected to the balanced action of the applied and eddy current fields, and the elastic reaction of the bowed walls. This model can be incorporated into the general concept of loss separation, by calculating the classical loss component through the solution of the Maxwell's diffusion equation under a magnetic constitutive law identified with the normal DC curve. The numerical domain wall model and the loss decomposition consistently predict that the excess loss component, playing a major role in these grain-oriented materials at power frequencies, tends to disappear in the upper induction-frequency corner.

83 1. Introduction

84 High-permeability grain oriented (HGO) Fe-Si sheets have slowly and steadily improved their magnetic
85 properties since their introduction in the seventies [1]. Better material purity and reduced density of defects,
86 domain refinement by laser scribing, and decreased sheet thickness without loss of crystallographic perfection
87 have been achieved along the years and products with power loss figure lower than 1.0 W/kg at 50 Hz and 1.7
88 T peak induction are nowadays available [2-4]. With present-day evolution in transformer applications, such
89 as those connected with the development of smart distribution grids and efficient power conversion in traction
90 [5, 6], where medium frequencies and non-sinusoidal voltages are involved, special interest is attached to the
91 use of the recently developed thin ($d = 0.18 - 0.20$ mm) HGO laminations. They appear ideal, for example, for
92 the working frequencies and induction waveforms of solid-state transformers and transformers employed in
93 DC-DC converters [7, 8]. However, by moving the frequencies in the kHz range, we are faced with novel
94 requirements regarding the precise characterization of the HGO sheets and of inductive cores [9, 10], whereas
95 solidly assessed concepts routinely applied in the theoretical interpretation of the magnetic losses at power
96 frequencies need to be revisited, in the light of a remarkable evolution of the dynamics of the domain walls
97 (dws) and the progressively reduced penetration of the magnetic flux across the sheet core. The question is
98 therefore posed regarding the way one can consistently fit the decrease of the skin depth in a mechanism for
99 the unfolding of the dw motion under increasing frequency and how this is quantitatively reflected in the
100 corresponding evolution of the energy loss $W(f)$. This quantity is theoretically assessed in GO sheets, up to
101 frequencies where the assumption of near-uniform flux through the sheet depth holds, by the Statistical Theory
102 of Losses (STL). It is a physical model, which provides a full interpretation, through the quantitative derivation
103 of the loss components, of the dependence of $W(f)$ on frequency and peak polarization J_p [11, 12]. Remarkably,
104 STL equally applies to non-oriented and grain-oriented steel sheets. Some criticism was raised in the recent
105 literature concerning the adopted simple formulation of the classical loss component $W_{\text{class}}(f)$ under standard
106 conditions (full flux penetration) and high J_p values [13, 14]. It was experimentally shown, however, that the
107 suggested alternative approach, the so-called saturation-wave-model, overestimated the measured loss in non-
108 oriented sheets [15], while it was originally demonstrated that, by treating the motion of the 180° dws in
109 statistical terms, distinct classical and excess $W_{\text{exc}}(f)$ contributions can always be identified in HGO sheets
110 [12]. It is apparent, in fact, that, even in the presence of well-defined arrays of 180° dws, one cannot get rid of
111 a statistical distribution of the pertaining variables in actual GO sheets. Renouncing to the separate
112 identification of $W_{\text{class}}(f)$ and $W_{\text{exc}}(f)$, as proposed in [14], can be seen as a possible alternative. However, the
113 prediction of the dynamic loss $W_{\text{dyn}}(f) = W_{\text{class}}(f) + W_{\text{exc}}(f)$ requires in this case a far from simple retrieval of J -
114 dependent fitting parameters from pre-emptive measurements. Of course, at frequencies sufficiently high to
115 hinder flux penetration, the following standard formulation for the classical loss (assuming induction and
116 polarization to coincide) in a lamination of thickness d and conductivity σ

$$117 \quad W_{\text{class}}(f) = \frac{\pi^2}{6} \sigma J_p^2 d^2 f \quad [\text{J/m}^3] \quad (1)$$

118 does not hold, as well as the closed expression obtained as solution of the Maxwell's diffusion equation in a
119 hypothetical linear medium of defined permeability μ

120
$$W_{\text{class}}(f) = \frac{\pi}{2} \frac{\gamma J_p^2}{\mu} \frac{\sinh \gamma - \sin \gamma}{\cosh \gamma - \cos \gamma}, \quad [\text{J/m}^3] \quad (2)$$

121 where $\gamma = \sqrt{\pi \sigma \mu d^2 f}$. The point becomes then one of finding $W_{\text{class}}(f)$ in the actual non-linear hysteretic
 122 material, an arduous objective, given that the solution of the diffusion equation coupled with a local dynamic
 123 hysteresis model, the method applied in non-oriented steel sheets [16, 17], is hardly applicable to the coarse
 124 dw array of the HGO materials. Whatever the case, the statistical treatment discussed in [12] inevitably leads
 125 to the decomposition $W_{\text{dyn}}(f) = W_{\text{class}}(f) + W_{\text{exc}}(f)$ in the GO sheets, including the case of orientations different
 126 from the rolling direction [18, 19]. In this work we shall simplify the matter by introducing the DC normal
 127 magnetization curve, taken as the magnetic constitutive equation of the material, in the electromagnetic
 128 diffusion equation and we shall calculate $W_{\text{class}}(f)$ accordingly. We shall associate the evolution of the dynamic
 129 losses versus f and J_p with stroboscopic Kerr observations of the surface domain structure. The Kerr
 130 experiments will provide a stringent test for the modeling of the dw dynamics, which will be carried out starting
 131 from the concept of dw bowing and its numerical implementation, for an array of equally spaced dws, bearing
 132 on Bishop's analysis of flexible, eddy current limited motion of single 180° dws [20, 21].

133 Various phenomenological-empirical formulations have been proposed in recent and less recent times for
 134 dealing with broadband losses in magnetic sheets, many of them relying on variously modified Steinmetz's
 135 equation and the ensuing search for a more-or-less relevant number of fitting parameters or on extended
 136 experimental characterization [22-25]. In the present work, where we investigate 0.174 mm and 0.289 mm
 137 thick sheets up to 10 kHz, we privilege the physical approach and the idea of loss decomposition, a concept
 138 preserving its meaning even in the presence of deep skin effect. The simulation of the behavior of the array of
 139 flexible dws upon increasing J_p and f permits one to predict the progressive transformation of the back-and-
 140 forth motion of the 180° dws (mode 1) into a moving horizontal front, separating a saturated band beneath the
 141 sheet surface from a nearly demagnetized inner core (mode 2), as sketched in Fig. 1. This justifies the
 142 correspondingly observed relative drop of $W_{\text{exc}}(f)$ in the upper (J_p, f) corner (e.g., 1.5 T at 5 kHz). A key role
 143 in such phenomena is evidently played by the sheet thickness.

144
 145 **2. Energy losses in HGO sheets up to 10 kHz and their interpretation**

146 Hysteresis loops and losses were measured, under controlled sinusoidal polarization, between 1 Hz and 10
 147 kHz on 0.174 mm and 0.289 mm thick HGO sheets. The polarization range 250 mT-1.7 T could be covered
 148 by combining Epstein frame and single strip testing. **The 200 turns Epstein frame (IEC standard 60404-10) has**
 149 **been used up to 1 kHz, and a single Epstein strip tester with using local field measurements (H-coil) has been**
 150 **preferred above the kilohertz, because such system allows a significant decrease of the required apparent power**
 151 **[26].** Individual strips were then prepared for dynamic magneto-optical analysis, which was performed by
 152 means of a stroboscopic setup on the strip subjected to defined exciting regime, the flux closure being ensured
 153 by a C-shaped laminated yoke. The domain structure was observed at selected points of the hysteresis loop on
 154 a 5 mm spot located on a well-oriented grain. Each image is obtained by averaging the individual frames and
 155 subtracting the background upon a few thousand successive cycles. The main features and the operating
 156 procedures of the employed fluxmetric and magneto-optical setups are fully discussed in [27].

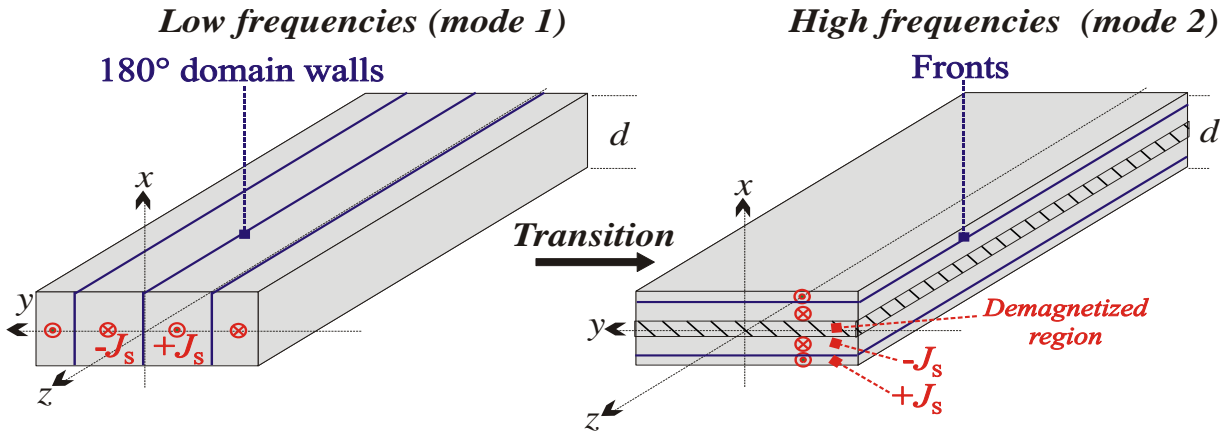


Fig. 1 – The back-and-forth motion of the 180° dws occurring at power frequencies in HGO sheets (mode 1) evolves under increasing frequency via dw bowing and eventual merging at the sheet surface into a magnetization reversal carried out by a front propagating from surface to sheet midplane (mode2).

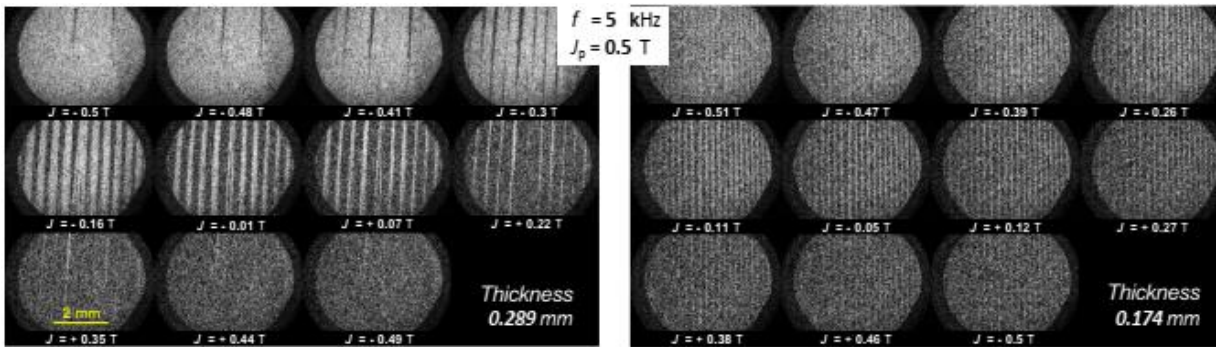


Fig. 2. Kerr imaging of the surface domain structure along a semi-cycle taken at 5 kHz and bulk peak polarization $J_p = 0.50$ T in the 0.289 mm and 0.174 mm thick HGO sheets. The surface peak polarization is estimated to attain the values 1.85 T and 1.3 T in the thicker and thinner strips, respectively. This quantity can fluctuate from grain to grain.

157 The standard analysis by the STL of the energy loss versus frequency behavior in HGO sheets permits
 158 one to recognize incipient skin effect by the failure of Eq. (1) in data fitting. This generally occurs, depending
 159 on the sheet thickness, beyond power frequencies. One can then observe by Kerr imaging that the surface J_{psurf}
 160 and the bulk J_p peak polarization values increasingly diverge under increasing f , till the point where, depending
 161 on J_p , the material saturates at the surface for a fraction of the semi-period. This effect is apparent in Fig. 2,
 162 where the evolution along a semi-cycle of the surface domain structure in the 0.289 mm and 0.174 mm thick
 163 sheets is shown for $f = 5$ kHz and $J_p = 0.50$ T. The skin effect is manifest here, embodied in the faster motion
 164 of the dws at the surface with respect to the bulk (dw bowing) and the partial disappearance of the surface
 165 domains at the tip points of this low- J_p cycle. By image analysis we get $J_{psurf} \sim 1.85$ T and $J_{psurf} \sim 1.3$ T in the
 166 thicker and thinner sheet, respectively. J_{psurf} will obviously saturate under increasing J_p . The problem is
 167 therefore posed regarding the overall dw evolution versus J_p and f and its modeling, which must be consistent
 168 with the Kerr observations and the macroscopic behavior of the GO sheets.

169 A. From domain wall bowing to the front-like mechanism

170 We assume a [001](110) infinitely extended single crystal endowed with regular anti-parallel 180° dws. At
 171 low frequencies the walls move back-and-forth under an alternating field, and can be assimilated, from the

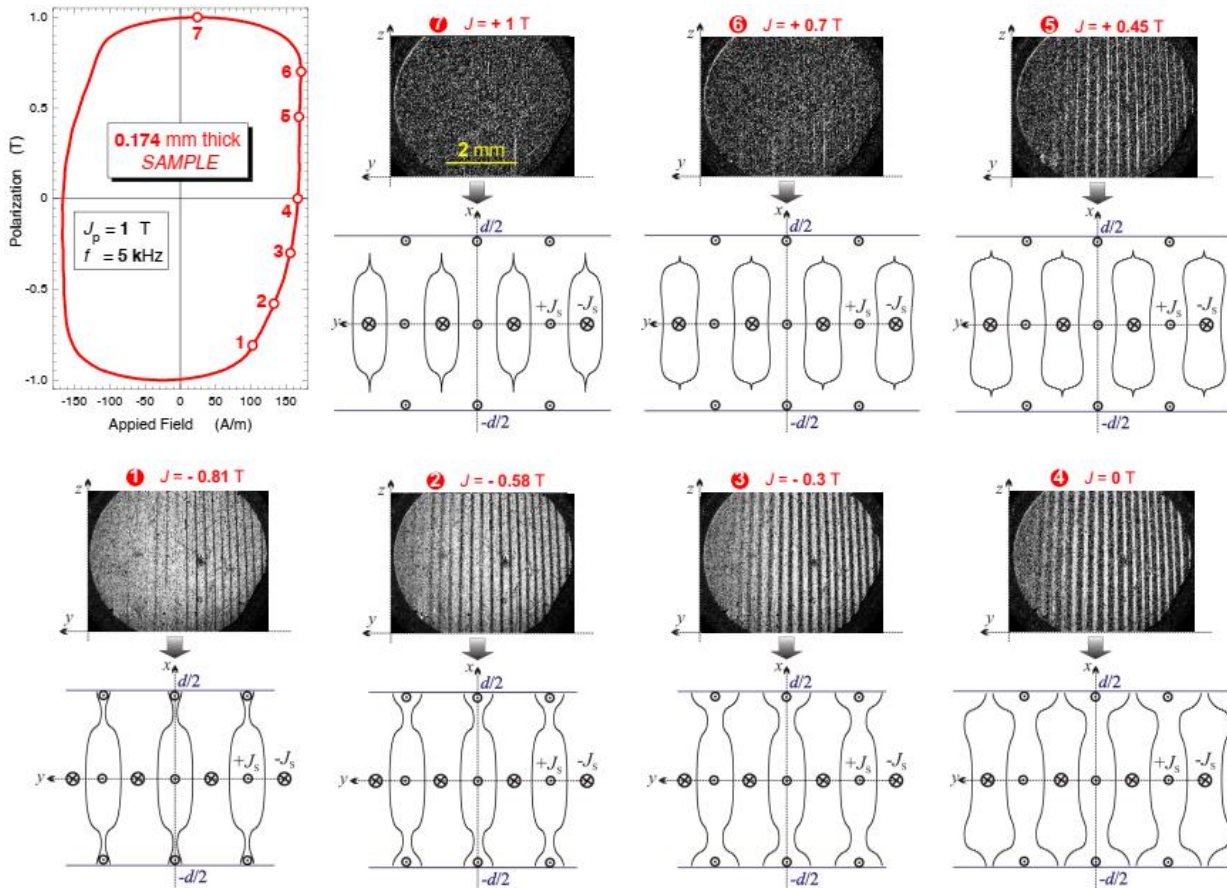


Fig. 3. 0.174 mm thick HGO sheet cyclically magnetized between ± 1.0 T at 5 kHz. The Kerr observation of the surface domain structure at different points of the ascending branch of the loop (y - z plane) is associated with a cross-sectional view (x -axis) of the corresponding evolution of the domain structure, as predicted by the numerical model of dw bowing.

172

173 viewpoint of their dynamic behavior, as rigid objects (Pry&Bean model [28]). The Kerr results provide direct
 174 evidence of strong dw bowing and dw merging at the surface for sufficiently high ($J_p f$) product. Such conditions
 175 are largely met in the present experiments, thereby calling for an appropriate model for the dw motion, which
 176 we developed, starting from the classical Bishop's model [20, 21], according to the following assumptions:

- 177 • The wall energy is $\gamma_w = 1.3 \cdot 10^{-3}$ J/m², and the electrical resistivity is $\rho = 48 \cdot 10^{-8}$ $\Omega \cdot m$. An
 178 infinite array of dws is considered, with spacing defined at each frequency by the Kerr observations.
- 179 • Each dw at rest is subdivided into $n = 128$ identical vertical elementary segments. The bowing
 180 of the dw under a changing applied field is then emulated, following Bishop's model, by connecting
 181 the vertical segments moving at different speed with horizontal segments, which allow for bowing by
 182 increasing their length on approaching the surface from the midplane. A dynamic balance is reached
 183 at any instant of time between the pressure exerted by the applied field and the counteracting effect by
 184 the eddy current field and the surface tension of the deformed wall. The eddy current field acting on
 185 any element is calculated by taking into account the contribution of the whole infinite array of equally
 186 moving 180° dws. The restoring force associated with the static coercivity does not play any role in
 187 this context. The mean dynamic dw spacing $2L$ is observed to decrease with the sheet thickness. We
 188 find, for example $2L \sim 0.24$ mm and $2L \sim 0.14$ mm in the 0.289 mm and 0.174 mm thick HGO sheets,

189 respectively, at 5 kHz.

- 190 • At sufficiently high values of the product ($J_p f$) the bowing is severe and the dws collide at
191 the sheet surface, where the magnetization tends to saturate (see Fig. 2). Further flux variation is
192 therefore ensured by the wall portions surviving in the bulk, which connect to form shrinking domains.
193 It is the natural evolution of the bowing mechanism, which has been implemented in the code.

194 Fig. 3 provides a sequence of Kerr images of the surface domain structure, taken on the 0.174 mm thick
195 sheet for $J_p = 1.0$ T and $f = 5$ kHz, at different points of the hysteresis loop. It is noted that the surface
196 magnetization saturates for $J = J_p$. Each image is accompanied by the cross-sectional view of the
197 correspondingly predicted profile of the domain structure ($-d/2 \leq x \leq d/2$), whose evolution along the ascending
198 branch of the loop compares with the measured bulk magnetization and the Kerr results. Fluxmetric results,
199 Kerr imaging, and theoretical prediction are shown to consistently fit in the example of Fig. 4, which deals
200 with the characterization of the 0.289 mm thick sheet at 1.5 kHz for $J_p = 1.5$ T. To note the comparison between
201 the Kerr images of the surface domains and the corresponding cross-sectional view of the theoretical domain
202 structure at the points A and B of the ascending branch of the experimental loop (open symbols). The scenario
203 is one pertaining to the upper (J_p, f) corner, where mode 2 is expected to prevail. The model shows that reverse
204 domains are nucleated at the sheet surface upon returning from J_p (point A). They expand further under
205 increasing reverse field, to eventually merge and cover the whole surface (point B), thereby forming a

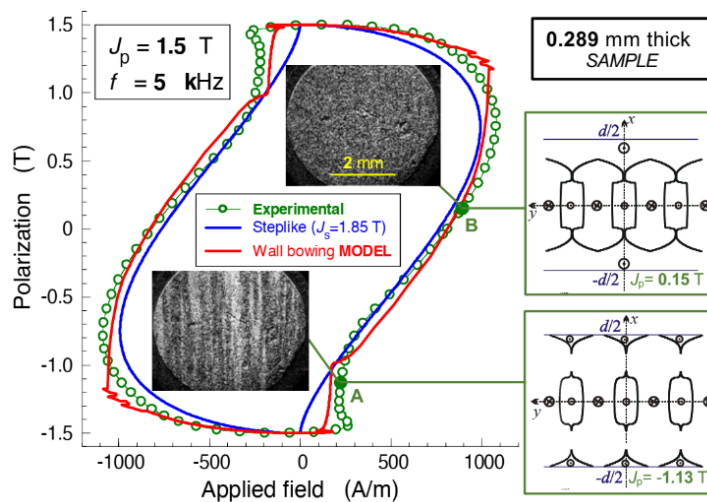


Fig. 4. 0.289 mm thick HGO sheet. The experimental cycle taken at $f = 5$ kHz for $J_p = 1.5$ T (open symbols) is compared with the loop calculated by the bowing model, accounting for wall periodicity and merging (red line), and the loop calculated according to the ideal case of step-like constitutive equation [12] (blue line). The surface domain structure by Kerr imaging associated with points A and B is compared with the cross-sectional view of the predicted domain structure.

206 downward moving boundary (a horizontal undulating 180° dw), in analogy with the scheme sketched in Fig.
207 1. By plotting the rated sinusoidal $J(t)$ against the sustaining applied field $H_a(t)$ entering the dynamic dw model,
208 we obtain substantial agreement with the experimental loop (red line in Fig. 4). To note that the quasi-static
209 hysteresis provides negligible loss contribution at this frequency, while the the corresponding loop at $J_p = 1.5$

210 T is nearly square. It appears therefore appropriate to recognize the extent to which a classical calculation
 211 assuming a step-like $J(H)$ constitutive equation, entailing a perfect mode 2 magnetization process, can estimate
 212 the actual dynamic hysteresis loop. It is a simplest approach, for which there is analytical solution [12], leading
 213 to the inner loop (blue line) in Fig. 4 and therefore providing an acceptable prediction, but for the region
 214 immediately following the reversal (point A), where a small extra-area appears. This is what we expect,
 215 because the Kerr effect and the bowing model show a certain dw activity there. We can conclude that most of
 216 the energy loss is lumped into the classical term W_{cl} (although not predictable by Eq. (1)), but the small
 217 contribution by W_{exc} cannot be ignored.

218 Similar results can be found in the thinner GO sheet, although at higher f and J_p values. The comparison of
 219 high frequency loops and losses given in Fig. 5 shows the great advantage of thinner sheets in terms of reduced
 220 losses. We shall prove in the following that this is mostly due to the strong decrease of $W_{class}(f)$.

221 **B. Loss separation**

222 We have previously stressed that the concept of classical loss $W_{class}(f)$ is physically justified in HGO sheets,
 223 despite their coarse domain structure. The difficult point remains, however, that of dealing with the actual non-
 224 linear hysteretic magnetic behavior of the material if $W_{class}(f)$ is to be calculated in the presence of skin effect.
 225 Some simplification should be attempted, by which one could connect, for example, the simple Eq. (1) at low

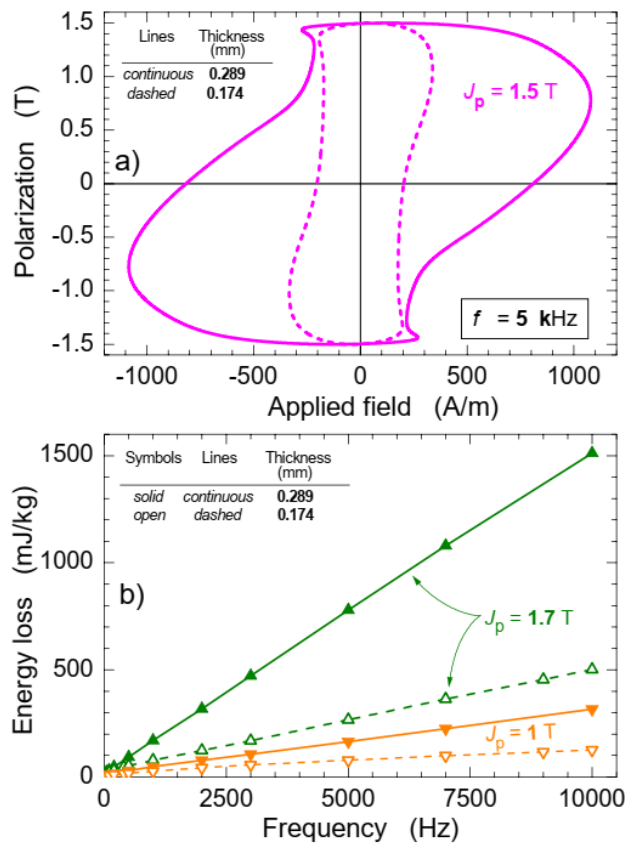


Fig. 5. (a) Hysteresis loops measured at 5 kHz in the 0.289 mm and in the 0.17 mm thick samples for $J_p = 1.5$ T. (b) Energy loss $W(f)$ measured up to 10 kHz in the same sheet samples for $J_p = 1.0$ T and $J_p = 1.7$ T.

226 frequencies with the step-like model at the highest polarization and frequency values. A possibility to cope
 227 with these two requirements is to define $W_{\text{class}}(f)$ as the quantity obtained by numerically solving the Maxwell's
 228 diffusion using the normal magnetization curve as the constitutive law of the material and determining a
 229 polarization profile $J(x)$ across the sample thickness [27]. The hysteresis loss component is then calculated by
 230 integrating $W_{\text{hyst}}(J(x))$, a quantity known from pre-emptive knowledge of the quasi-static loss upon an
 231 appropriately wide polarization range. Because of the non-uniform profile of $J(x)$, $W_{\text{hyst}}(J_p)$ is predicted to

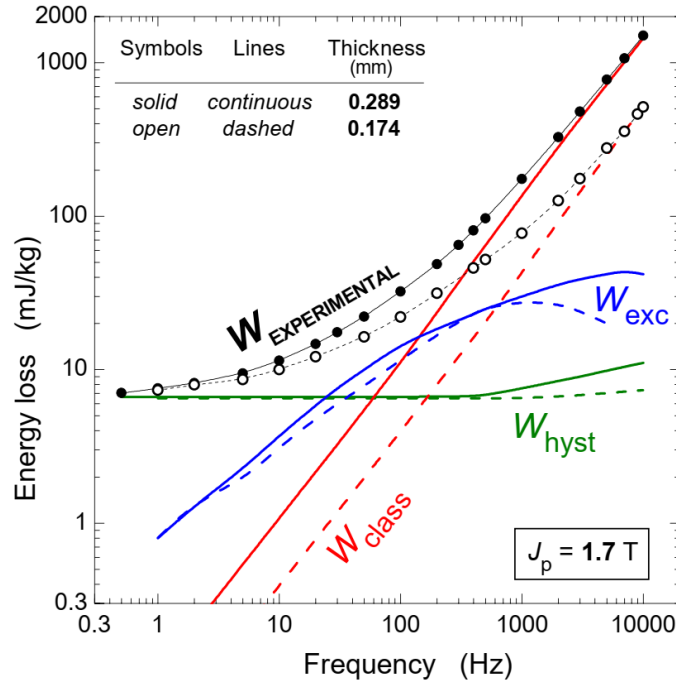


Fig. 6. Loss separation performed at 1.7 T up to 10 kHz in the 0.289 mm and 0.174 mm thick HGO sheets. The decrease of the measured $W(f)$ observed at high frequencies in the thinner sheets (see also Fig. 5b) is largely due to the corresponding decrease of $W_{\text{class}}(f)$, here calculated by taking the normal DC magnetization curve as the magnetic constitutive equation of the material. The hysteresis component W_{hyst} is predicted to increase at high frequencies, but it becomes, at the same time, inessential. $W_{\text{exc}}(f)$ shows instead a markedly restrained increase beyond a few hundred Hz, following the transition of the magnetization process from mode 1 to mode 2.

232 increase with f in the presence of skin effect. This could result into a somewhat overestimated $W_{\text{hyst}}(J_p)$ in the
 233 upper (J_p, f) corner, where the dw processes play a minor role (see Fig. 4). However, it is apparent in Fig. 6
 234 that the contribution of $W_{\text{hyst}}(J_p)$ to $W(f)$ becomes in any case irrelevant. The excess loss $W_{\text{exc}}(f)$ is eventually
 235 obtained, for any J_p value, as the difference $W_{\text{exc}}(f) = W(f) - W_{\text{hyst}}(f) - W_{\text{class}}(f)$. The so-obtained loss
 236 decomposition, shown up to 10 kHz for $J_p = 1.7$ T in Fig. 6, shows that the large decrease of $W(f)$ observed in
 237 the thinner sheet at high frequencies (Fig. 5) chiefly comes from a corresponding decrease of $W_{\text{class}}(f)$. It is
 238 associated with the transition of the magnetization process from mode 1 to mode 2, where the role of the dws,
 239 mainly connected with the domain nucleation at the point of reversal, becomes residual. $W_{\text{exc}}(f)$
 240 correspondingly deviates from the low-frequency power law $W_{\text{exc}}(f) \propto f^n$, with $n \sim 0.6$, and flattens out, an
 241 effect occurring sooner in the thicker sheet.

243 From mode 1 to mode 2: some details

244 We have shown that the transformation of the magnetization process from mode 1 to mode 2 is completed
245 in the upper (J_p, f) corner. At low J_p and f values, the walls do not merge, while at sufficiently high frequencies
246 a J_p value exists, for which two neighboring walls come in contact at their tip points at the sheet surface. By
247 further increasing J_p , the walls merge and the sheet saturates across a horizontal band, thereby forming a
248 domain arrangement reminding of the ideal mode 2 structure (see Fig. 4). An inner array of pseudo-elliptical
249 domains, shrinking under the expanding horizontal band, ensures the existence of a near demagnetized region
250 across the sheet core. At any frequency, the calculated fraction $\Delta t/T$ of the time period where the surface
251 remains in the saturated state is predicted to increase with J_p , as shown in Fig. 7 (dashed lines). For a defined
252 $\Delta t/T$ value, J_p and f follow an inverse relationship, where the hyperbolic parameter $k(\Delta t/T) = J_p f$ is observed to
253 be larger, by virtue of the reduced eddy currents, in the thinner sheets. A few experimental points are provided
254 in Fig. 7, where the (J_p, f) pairs identify $W_{exc}(f)$ values lower than 10 % of the dynamic losses. With ($\Delta t/T$)
255 occupying more than 60 % of the period, $W_{exc}(f)$ tends to disappear.

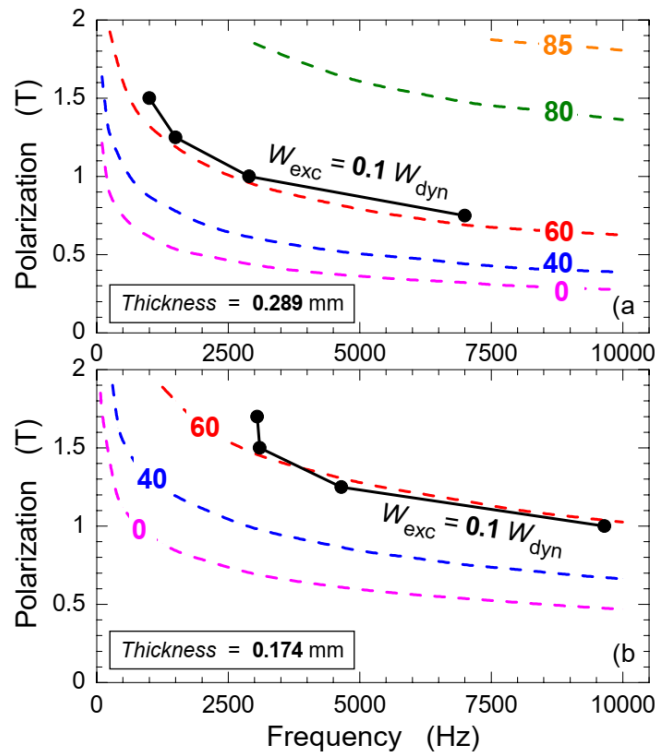


Fig. 7. The dashed lines show in percentage the calculated proportion of the magnetization period where the sheet surface is magnetically saturated (beneath the 0 line, no wall contact can occur). The solid line connects the (J_p, f) experimental points where the excess loss $W_{exc}(f)$ is reduced to 10 % of the dynamic loss. It is noted how the (J_p, f) corner moves upward in the thinner sheets.

256 **3. Conclusions**

257 HGO Fe-Si sheets have been characterized up to 10 kHz by means of fluxmetric measurements and direct
258 observations of the dw dynamics by stroboscopic Kerr investigations. The role of sheet thickness has been
259 investigated by comparing the loss versus frequency behavior of 0.289 mm and 0.174 mm thick samples. The

260 decomposition of the measured loss $W(f)$ has been carried out for a range of peak polarization values J_p and
261 evolving degree of flux penetration with frequency, which prevents the overall application of the standard
262 formulation for the classical loss component $W_{\text{class}}(f)$. The Maxwell's diffusion equation has therefore been
263 numerically solved by taking the normal magnetization curve as the magnetic constitutive equation of the
264 material, thereby connecting in a continuous fashion low- and high-frequency response. A minor-to-marginal
265 role by the dw-generated loss contributions (hysteresis and excess components) is thus predicted to occur, in
266 all cases, beyond a few kHz. Consequently, the large decrease shown by $W(f)$ at high frequencies on passing
267 from the 0.289 mm to the 0.174 mm thick sheets is chiefly associated with a corresponding decrease of $W_{\text{class}}(f)$.
268 We consistently provide a microscopic interpretation of the loss phenomenology by focusing on the dw
269 behavior, exploiting dynamic Kerr observations of the domains at the sheet surface, together with the modeling
270 of the 180° wall motion. This is based on the notion of dw bowing and it permits one to provide a dynamic
271 picture of the array of dws, where, on attaining the high (J_p, f) corner, the low-frequency back-and forth 180°
272 dw oscillations (mode 1) pass through the merging of neighboring walls at the sheet surface and the creation
273 of subsurface symmetric saturated horizontal bands, whose boundaries move towards the demagnetized sheet
274 core under changing applied field. This is in rough analogy with the ideal magnetization mode 2, the one
275 envisaged for a step-like $J(H)$ constitutive equation.

276

277 **Funding:** This research work was partially supported by the 19ENG06 HEFMAG project, which was funded by the
278 EMPIR program, and co-financed by the Participating States and the European Union's Horizon 2020 research and
279 innovation program.

280

281 References

282

- 283 [1] S. Taguchi, T. Yamamoto, A. Sakakura, New grain-oriented silicon steel with high permeability "ORIENTCORE
284 HI-B", *IEEE Trans. Magn.* 10 (1974), 123-127 <https://doi.org/10.1109/TMAG.1974.1058316>.
- 285 [2] Y. Ushigami, M. Mikozami, M. Fujikura, T. Kubota, H. Fujii, K. Murakami, "Recent development of low-loss grain-
286 oriented silicon steel, *J. Magn. Magn. Mater.* 254–255 (2003) 307–314. [https://doi.org/10.1016/S0304-
287 8853\(02\)00933-2](https://doi.org/10.1016/S0304-8853(02)00933-2).
- 288 [3] Z. Xia, Y. Kang, Q. Wang, Developments in the production of grain-oriented electrical steel, *J. Magn. Magn. Mater.*
289 320 (2008) 3229-3233. <https://doi.org/10.1016/j.jmmm.2008.07.003>.
- 290 [4] S. Takajo, T. Ito, T. Omura et S. Okabe, Loss and noise analysis of transformer comprising grooved grain-oriented
291 silicon steel, *IEEE Trans. Magn.* 53 (2017) 2001606. <https://doi.org/10.1109/TMAG.2017.2710039>.
- 292 [5] Q. Huang, M.L. Crow, G.T. Heydt, J. P. Zheng, and S. J. Dale, The future renewable electric energy delivery and
293 management (FREEDM) system: The energy internet, *Proc. IEEE* 99 (2011)133–148.
294 <https://doi.org/10.1109/JPROC.2010.2081330>.
- 295 [6] C. Zhao, D. Dujic, A. Mester, J. K. Steinke, M. Weiss, S. Lewdeni-Schmid, T. Chaudhuri, and P. Stefanutti, Power
296 Electronic Traction Transformer—Medium Voltage Prototype, *IEEE Trans. Ind. Electr.* 61 (2014) 3257-3268.
297 <https://doi.org/10.1109/TIE.2013.2278960>.
- 298 [7] M.A. Hannan, P.J. Ker, M.H. Lipu, Z.H. Choi, M.S.A. Rahman, K.M. Muttaqi, and F. Blaabjerg, State of the art of
299 solid state transformers: advanced topologies, implementations issues, recent progress and improvements, *IEEE*
300 *Access*, 8 (2020) 19113 – 19132. <https://doi.org/10.1109/ACCESS.2020.2967345>.
- 301 [8] N. Soltau, D. Eggers, K. Hameyer, and R. W. De Doncker, Iron losses in a medium-frequency transformer operated
302 in a high-power DC–DC Converter, *IEEE Trans. Magn.* 50 (2014) 7023604.
303 <https://doi.org/10.1109/TMAG.2013.2283733>.
- 304 [9] T. Belgrand, R. Lemaître, A. Benabou, J. Blaszkowski, and C. Wang, Thin grain oriented electrical steel for PWM
305 voltages fed magnetic cores, *AIP Advances* 8 (2018) 047611. <https://doi.org/10.1063/1.4993712>.
- 306 [10] H. Ichou, D. Roger, M. Rossi, T. Belgrand et R. Lemaître, Assessment of a grain oriented wound core transformer
307 for solid state converter, *J. Magn.Magn. Mater.* 504, (2020) 166658. <https://doi.org/10.1016/j.jmmm.2020.166658>.

- 308 [11] G. Bertotti, General properties of power losses in soft ferromagnetic materials, *IEEE Tran. Magn.* 24 (1988) 621-
309 630. <https://doi.org/10.1109/20.43994>
- 310 [12] G. Bertotti, *Hysteresis in Magnetism*, San Diego, CA, Academic Press, 1998.
- 311 [13] S. Steentjes, S.E. Zirka, Y.I. Moroz, E.Y. Moroz, and K. Hameyer, Dynamic magnetization model of nonoriented
312 steel sheets, *IEEE Tran. Magn.* 50 (2014) 621-630. 7300204. <https://doi.org/10.1109/TMAG.2013.2284357>.
- 313 [14] S.E. Zirka, Y.I. Moroz, S. Steentjes, K. Hameyer, K. Chwastek, S. Zurek, and R.G. Harrison. Dynamic
314 magnetization model for soft ferromagnetic materials with coarse and fine domain structure, *J. Magn.Magn. Mater*
315 394, (2015) 229-236. <http://dx.doi.org/10.1016/j.jmmm.2015.06.082>.
- 316 [15] C. Ragusa, H. Zhao (赵滄宇), C. Appino, M. Khan, O. de la Barrière, and F. Fiorillo, Loss decomposition in non-
317 oriented steel sheets: the role of the classical losses, *IEEE Magn. Lett.* 7 (2016) 5106105.
318 <https://doi.org/10.1109/LMAG.2016.2604204>.
- 319 [16] V. Basso, G. Bertotti, O. Bottauscio, M. Chiampi, F. Fiorillo, M. Pasquale, and M. Repetto, Power losses in magnetic
320 laminations with hysteresis: finite element modelling and experimental validation, *J. Appl. Phys.* 81 (1997), 5606 –
321 5608. <https://doi.org/10.1063/1.364614>.
- 322 [17] L. Dupré, O. Bottauscio, M. Chiampi, M. Repetto et J. Melkebeek, Modeling of electromagnetic phenomena in soft
323 magnetic materials under unidirectional time periodic flux excitations, *IEEE Trans. Magn.* 35 (1999) 4171-4184.
324 <https://doi.org/10.1109/20.799065>.
- 325 [18] C. Appino, E. Ferrara, F. Fiorillo, C. Ragusa, and O. de la Barrière, Static and dynamic energy losses along different
326 directions in GO steel sheets, *J. Magn. Magn. Mater.* 500 (2020) 166281.
327 <https://doi.org/10.1016/j.jmmm.2019.166281>.
- 328 [19] E. Ferrara, C. Appino, C. Ragusa, O. de la Barrière, and F. Fiorillo, Anisotropy of losses in grain-oriented Fe-Si,
329 *AIP Adv.* 11, (2021), 115208. <https://doi.org/10.1063/5.0066131>.
- 330 [20] J.E.L. Bishop, Understanding magnetization losses in terms of eddy current dominated domain wall dynamics, *J.*
331 *Magn.Magn. Mater.* 19 (1980) 336-344. [https://doi.org/10.1016/0304-8853\(80\)90626-5](https://doi.org/10.1016/0304-8853(80)90626-5).
- 332 [21] J.E.L. Bishop, Modelling domain wall motion in soft magnetic alloys, *J. Magn.Magn. Mater.* 41 (1984) 261-271.
333 [https://doi.org/10.1016/0304-8853\(84\)90193-8](https://doi.org/10.1016/0304-8853(84)90193-8).
- 334 [22] O. Messal, A. Kedous-Lebouc, O. Geoffroy, P. Mas, H. Dhahbi, C. Chillet, S. Buffat, and S. Randl, Analysis of the
335 Dynamic Behavior of Magnetic Materials Under High B and dB/dt. *Soft Magnetic Materials Conference SMM23*,
336 Sept. 2017, Séville, Spain (<hal-01589353>).
- 337 [23] J. Müllethaler, J. Biela, J.W. Kolar, J.W.; Ecklebe, A. Improved core loss calculation for magnetic components
338 employed in power electronic systems. *IEEE Trans. Power. Electron.* 2012, 27, 964–973.
339 <https://doi.org/10.1109/TPEL.2011.2162252>.
- 340 [24] W. Guan, H. Kong, M. Jin, L. Lan, Z. Du, Y. Zhang, J. Ruan, and H. Zhang, Analysis of excess loss in SiFe
341 laminations considering eddy-current dominated domain wall motion, , *IEEE Trans. Magn.* 51 (2015) 6300604.
342 <https://doi.org/10.1109/TMAG.2014.2362999>.
- 343 [25] B. Ducharme, P. Tsafack, Y.A. Tene Deffo, B. Zhang, and G. Sebald, Fractional operators for the magnetic dynamic
344 behavior of ferromagnetic specimens: an overview, *AIP Adv.* 11, (2021), 035309.
345 <https://doi.org/10.1063/90000044>.
- 346 [26] O. de la Barrière, C. Ragusa, M. Khan, C. Appino, F. Fiorillo, F. Mazaleyrat, A simple compensation method for the
347 accurate measurement of magnetic losses with a single strip tester, *IEEE Transactions on Magnetics*, vol.52 (2016),
348 No.5, pp. 1-4
- 349 [27] A. Magni, A. Sola, O. de la Barrière, E. Ferrara, L. Martino, C. Ragusa, C. Appino, and F. Fiorillo, Domain
350 structure and energy losses up to 10 kHz in grain-oriented Fe-Si sheets,” *AIP Adv.*, 11 (2021) 015220.
351 <https://doi.org/10.1063/9.0000184>.
- 352 [28] R. H. Pry and C. P. Bean, Calculation of the energy loss in magnetic sheet materials using a domain model, *J.*
353 *Appl. Phys.* 29 (1958) 532-533. <https://doi.org/10.1063/1.1723212> .